Effects of ion beam on the electrical conductivity and surface characteristics of flexible PVA/TiO_2 polymeric nanocomposites films

R. Altuijri[a], M. R. El-Aassar[b], A. Atta[c,*], M. M. Abdelhamied[d]
[a]*Department of Physics, College of Science, Princess Nourah bint Abdulrahman University, P.O. Box 84428, Riyadh 11671, Saudi Arabia.*
[b]*Chemistry Department, College of Science, Jouf University, P.O. Box: 2014, Sakaka, Saudi Arabia*
[c]*Physics Department, College of Science, Jouf University, P.O. Box: 2014, Sakaka, Saudi Arabia*
[d]*Radiation Physics Department, National Center for Radiation Research and Technology (NCRRT), Egyptian Atomic Energy Authority (EAEA), Cairo, Egypt*

The present research examined the impacts of oxygen beam bombardment on PVA/TiO_2 composites using cold cathode source with fluencies (3×10^{16}, 6×10^{16} and 9×10^{16} ions/cm^2). The X-ray diffraction (XRD) is verified the successful fabrication of PVA/TiO_2 composites. In addition, surface free energy, work of adhesion, and contact angles were evaluated for both pure and treated PVA/TiO_2 films. The drop in water contact angle from 68.37º to 52.12º was caused by an increase in ion beam fluence from 3×10^{16} ions/cm^2 to 9×10^{16} ions/cm^2. And the surface energy increases from 41.45 to 55.97 mJ/m^2, with a rise in the adhesion work from 98.75 mJ/m^2 to 116.33 mJ/m^2. In addition, the electrical conductivity of PVA/TiO_2 was measured within the frequency range of 50-10^6 Hz. After the samples subjected to 9×10^{16} ions/cm^2, the conductivity of the PVA/TiO_2 composite rose from 0.32×10^{-6} to 4.3×10^{-6} S/cm. The outcomes data showed that the electrical conductivity of the irradiated films were improved, which is important for different devices such batteries and supercapacitors.

(Received March 22, 2024; Accepted June 13, 2024)

Keywords: Polymer composite, Irradiation, Surface modifications, Material characterizations

1. Introduction

Polymeric composites have emerged as excellent material with novel surface properties across a wide range of industries due to their extensive functional properties [1]. Composites materials were grow up as new avenues of inquiry and potential solutions in many different applications [2, 3]. Surface wettability is one reason that polymer nanocomposites are used in printed electronics [4]. Modified surface wettability has numerous applications; it can enhance the strength and durability of adhesives used in woodworking, papermaking, and packaging, among many others. The electrical conductivity of polymer matrices can be enhanced by coating them with conductive nanoparticles [5].

Polymer materials with improved their structural characteristics are the basis for using in different applications [6]. PVA is can applied in a wide range of applications by modifying their properties like molecular weight and degree of hydrolysis [7]. As a hydrolyzable crystalline polymeric in water, PVA is excellent building block for other biopolymers [8]. Because of its hydrophilic nature, PVA can be cross-linked using several ways [9]. The low cost and high hydrophilicity of membranes based on PVA make them appealing for a variety of applications [10].

* Corresponding author: aamahmad@ju.edu.sa
https://doi.org/10.15251/DJNB.2024.192.941

Nanoparticles of titanium dioxide (TiO_2) are particularly noteworthy among these because of their many useful uses in a variety of fields and their one-of-a-kind qualities [11, 12]. The remarkable photocatalytic activity of TiO_2 nanoparticles is one of its distinguishing characteristics. [13]. The ability to use solar energy to catalyze chemical reactions is a remarkable attribute of TiO_2, which makes it highly desirable for uses like water purification and self-cleaning surfaces [14]. The large surface area-to-volume ratio of TiO_2 nanoparticles increases their reactivity and provides additional interaction sites [15]. This property is highly beneficial in the fields of catalysis, sensing, and composite material reinforcement [16].

Improving the characteristics of the nanocomposites is a result outcome of surface modifications that induced by ion beam irradiation [17]. Certain types of radicals are produced during ion beam treatment. Ion beam-treated polymer composites modify their electrical conductivity and surface characteristics to make them more useful for optoelectronic devices [18]. One way to make polymer composites more biocompatible is to modify their surface using ion beam irradiation [19].

The goal of this work is to fabricate flexible nanocomposites with unique properties for use in various devices. In this experiment, the composites were exposed to oxygen beams of varying fluencies. The impacts of ion beam on the physical characteristics of the fabricated films will be studied to direct these irradiated samples for used in different applications as coating, printing and supercapacitors.

2. Experimental method

The PVA solution was created by continuous stirring of the powder PVA for 2 hours and 78 °C in deionized water, and then mixed by 80 mL of acetic acid solution overnight. The solutions were combined and the mixture was stirred for 6 hours to produce the polymeric combination as analyzed before [20]. The polymer then mixed by TiO_2 to prepare PVA/TiO_2 as previously discussed [21]. The mixture of polymers and the composites were casted in the glass petri dish. The thickness was measured by a Mitutoyo (731 gauge) in the range of 60 um. The XRD (XRD 6000, Shimadzu, Japan) in the 2θ range of 5º to 85º is used to assess the structural. The morphology of the films were recorded by AFM (JEOL, Japan). The LCR (RS-232C) was applied to determine the conductivity in frequency 20 Hz to 5.2 GHz. To find the surface free energies, the contact angles was measured using of two liquids, distilled water and diiodomethane.

The films were exposed to ion beam as seen in the figure of ion source (Figure 1), at fluencies of $3x10^{16}$, $6x10^{16}$, and $9x10^{16}$ ions.cm^{-2}. The parts of the source are the extraction and ionizations regions, as previously discussed [22]. The beam extracted with pressure $1.6x10^{-4}$ mbar, current 130 μA/cm^2, and energy 4 keV.

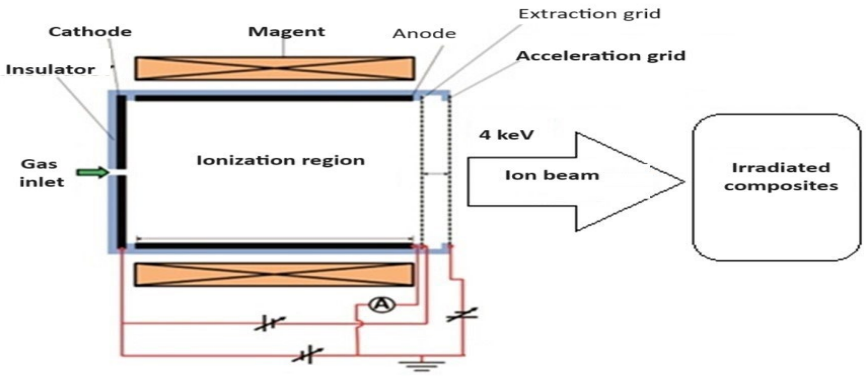

Fig. 1. A diagram of the modified cold cathode ion source.

3. Results and discussion

The SRIM simulation is applied to simulate the produced collisions information as ionizations, displacement and vacancies [23] of collided oxygen ions with PVA/TiO_2, as shown in Figure 2. The produced ionization of energy 4 keV is reacting with the PVA/TiO_2 at depth of 0 to 1000 A^o as shown in Figure 2a. An atom breaks free from its location and accelerates away from the parent macromolecule. The atom stops between polymer macromolecules after collisions and kinetic energy loss. The damage to targets occurs because of ion collisions as investigated in Figure 2(b).

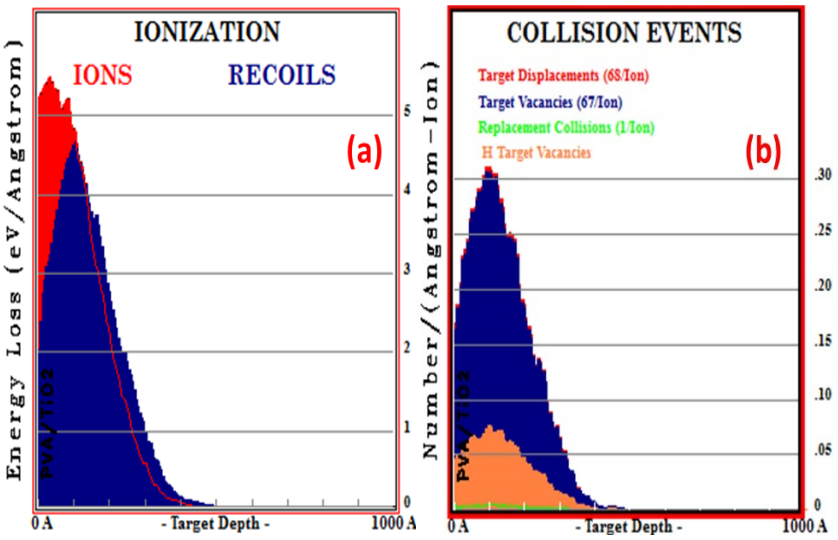

Fig. 2. (a) Ionization events and (b) collision of oxygen with PVA/TiO_2.

Figure 3 displays the XRD of the original and bombarded PVA/TiO_2. The PVA polymer was revealed to be semi-crystalline in the XRD, with a height peak 19.94° suggesting PVA structure. TiO_2 exhibited a diffraction peak at 25.8° associated to (111). Furthermore, a change in PVA peak with intensities showed crystallinity because of TiO_2 interacting in the PVA. As the ion beam increased, the defects inhaled into a crystal's structure induced recombination of electrons and holes. Moreover, it is noted that scission and radical production cause the PVA/TiO_2 peak amplitude to decrease with ion beam. Furthermore, the generation of free radicals and defect lead to the formation of orderly structure upon radiation, are responsible for the decrease in the (111) plane of PVA intensity. Additionally, after being exposed to ion beam, it can detect a shifting of the major peaks, which is brought on by strain on the lattice, and the formation of an internal defect. The crystallite size (D) of untreated and modified films is given by [24]:

$$D = \frac{0.94\lambda}{\beta \cos\theta} \tag{1}$$

The β is the width of (111) plane, the diffraction Bragg angle is θ, and the wavelength is indicated by λ. The following formula [25] is applied to get the diameter (R) by:

$$R = \frac{\lambda}{\sin\beta \cos 2\theta} \tag{2}$$

According to Table 1, the value of D of TiO_2 for PVA/TiO_2 is 18.5 nm; and after exposed to 0.9×10^{17} ions/cm^2, it drops to 14.3 nm. While, R drops from 244.6 µm to 190.3 µm. The irradiation samples developed a disordered structure, which led to these outcomes. Using the following equation [25], the dislocation density (δ) was calculated by:

$$\delta = \frac{1}{D^2} \tag{3}$$

By exposure to radiation, the dislocation value for PVA/TiO_2 rose from 3.38×10^{-3} lines/m^2 to 6.06×10^{-3} lines/m^2. The lattice strain (ε) is computed by [25].

$$\varepsilon = \frac{\beta}{4\tan\theta} \tag{4}$$

After treatment, the ε rose from 0.081×10^{-3} for the virgin PVA/TiO_2 to 0.109×10^{-3}. Particle displacement following ion irradiation and a decrease in particle size are the causes of this alteration. Next, utilizing the next relationship [26] to determine the distorted parameters (g) by [26].

$$g = \frac{\beta}{\tan(\theta)} \tag{5}$$

After treatment, g increases from 12.05% in the unmodified PVA/TiO_2 film to 17.87%. This indicates ion irradiation modifies the crystalline behavior without altering the alignment of the crystals, hence inducing changes on the structure.

Table 1. Structural parameters of the PVA/TiO_2.

The samples	D [nm]	R [μm]	δ [10^{-3} lines/m^2]	ε [10^{-3}]	g (%)
PVA/TiO_2	18.5	244.6	3.38	0.081	12.05
3x10^{16} ions.cm^{-2}	17.1	228.7	3.56	0.092	12.44
6x10^{16} ions.cm^{-2}	15.2	204.1	5.49	0.103	15.52
9x10^{16} ions.cm^{-2}	14.3	190.3	6.06	0.109	17.87

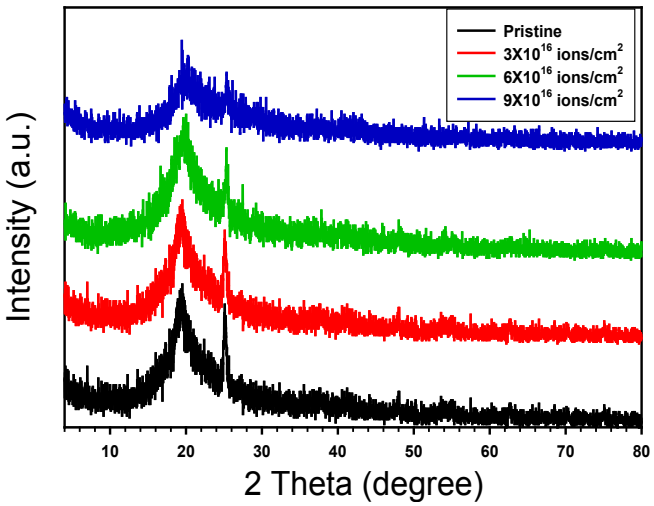

Fig. 3. XRD spectrum of PVA/TiO_2 films.

Figure 4a and 4b presented three-dimensional AFM topographical of PVA/TiO_2. It is observed that the incorporation of TiO_2 into polymer leads to an augmentation in surface roughness. The PVA//TiO_2 composite, which has undergone irradiation, exhibits increased surface roughness, thereby enhancing its suitability for various applications [27]. The roughness increases from 22 nm for PVA/TiO_2 to 35 nm for the irradiated composite by 9x10^{16} ions.cm^{-2}.

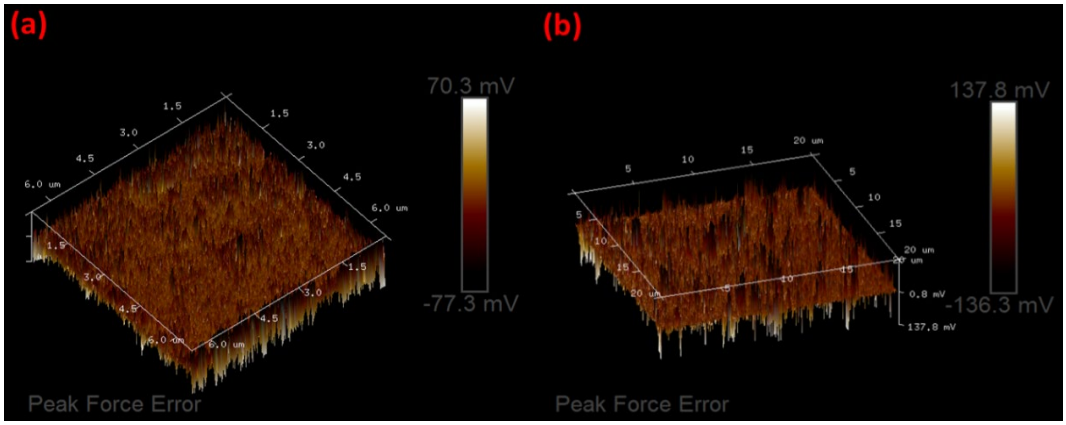

Fig. 4. 3D images of (a) PVA/TiO_2 and (b) treated PVA/TiO_2.

Figure 5(a–d) shows the morphology of PVA/TiO_2. In Figure 5(a), granular morphology with white dots spread on the film surface. Figure 5 (b-d) also displays SEM of PVA/TiO_2 irradiated by $3x10^{16}$, $6x10^{16}$, and $9x10^{16}$ ions/cm^2. Upon exposure, the polymer chains react with the TiO_2, as investigated by the SEM images. This reaction is attributed to the generation of numerous film defects and scission chains induced by the irradiation [28].

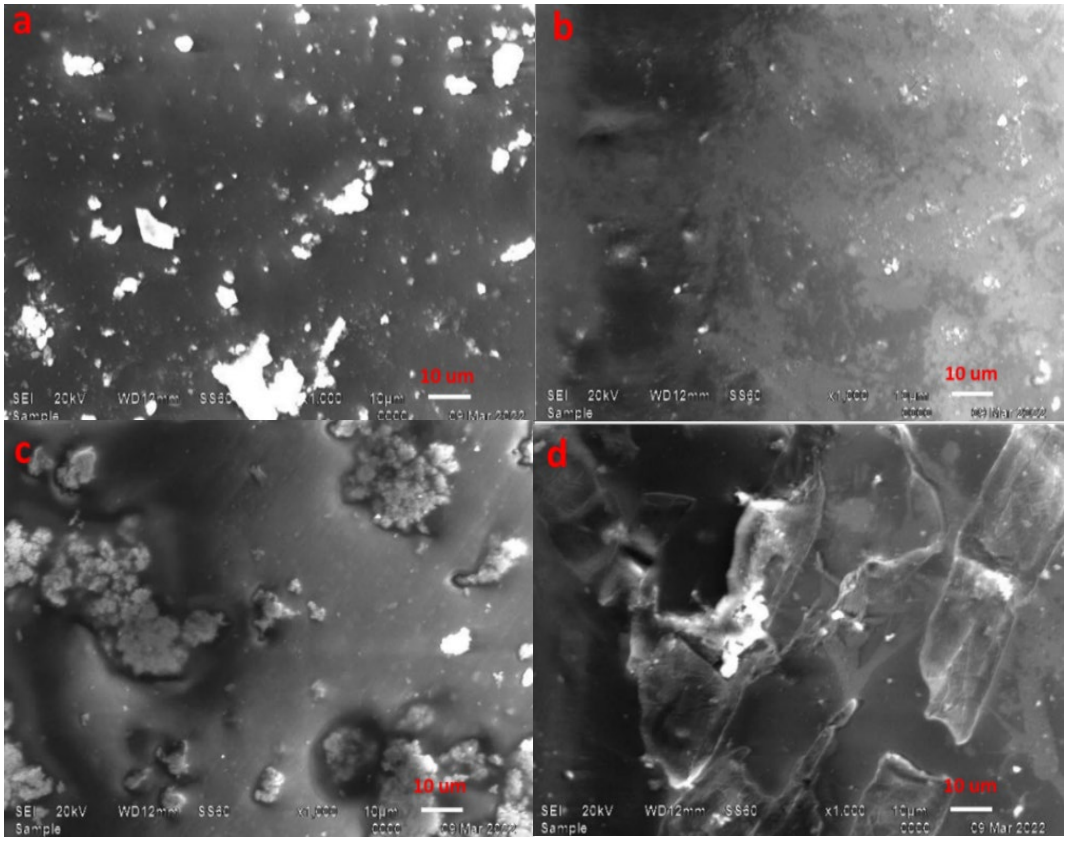

Fig. 5. SEM images of (a) untreated PVA/TiO_2 film and treated PVA/TiO_2 films with (b) $3x10^{16}$, (c) $6x10^{16}$, and (d) $9x10^{16}$ ions/cm^2.

The contact angles of PVA/TiO_2 are displayed in Figure 6. By increasing fluence, the contact angle is reduced. This because, the function groups forming on the hydrophobicity interface of PVA/TiO_2. When, ion fluence increases from 3x10^{16} ions/cm^2 to 9x10^{16} ions/cm^2, the water angle reduced from 68.37° to 52.12°, while the diiodomethane contact angle declined from 58.95° to 43.35°, as seen in Table 2. The angle is smaller for all treated materials when contrasted to pristine films [29].

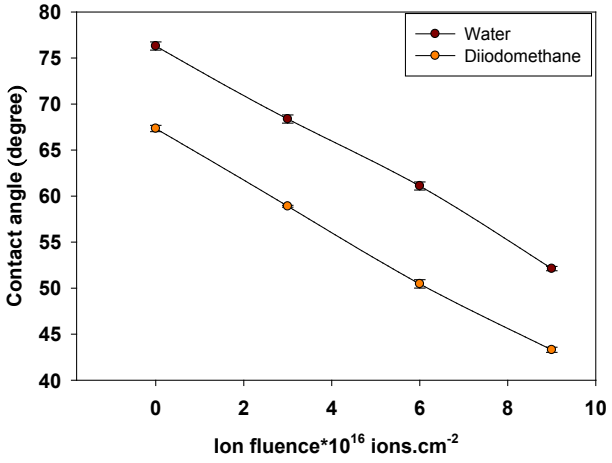

Fig. 6. Contact angle for PVA/TiO_2 films at different ion fluencies.

The adhesion work W_a with liquid free energy γ_l can be determined by [30].

$$W_a = \gamma_l(1 + \cos\theta) \tag{6}$$

The relation in Figure 7 shows the W_a with the ion treatment. As recorded in Table 2, the W_a increases from 98.75 mJ/m^2 to 116.33 mJ/m^2 for water liquid, and from 77.03 to 87.77 mJ/m^2 for diiodomethane, by increase in ion flux from 3x10^{16} ions/cm^2 to 9x10^{16} ions/cm^2. The change in adhesion work with different liquid polarities is caused by the changes in the surface hydrophilicity [31].

Table 2. The θ and W_a for PVA/TiO_2 at different ion fluencies.

The samples	θ (degree)		W_a (mJ/m^2)	
	Water	Diiodomethane	Water	Diiodomethane
PVA/TiO_2	76.30	67.34	89.17	70.37
3x10^{16} ions.cm^{-2}	68.37	58.95	98.75	77.03
6x10^{16} ions.cm^{-2}	61.13	50.46	106.74	83.13
9x10^{16} ions.cm^{-2}	52.12	43.35	116.33	87.77

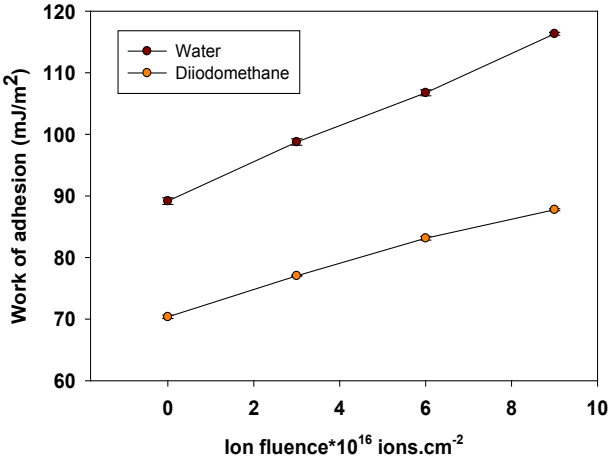

Fig. 7. The work of adhesion for PVA/TiO_2 films at different ion fluencies.

To determine the unknown value, the polar (γ_s^p) and the dispersive (γ_s^d) surface energy of PVA/TiO_2 , is using the relation of the tensions of solid-liquid γ_{sl} and the tension of solid-vapourγ_s, and liquid-vapour γ_l by equation 7 [32].

$$\frac{\gamma_l(1+\cos\theta)}{2\sqrt{\gamma_l^d}} = \sqrt{\gamma_s^d} + \sqrt{\gamma_s^p}\cdot\sqrt{\frac{\gamma_l^p}{\gamma_l^d}} \tag{7}$$

The changes in dispersive γ_s^d, the polar γ_s^p, and total γ_s^t for pure and irradiated PVA/TiO_2 is given in Figure 8. As recorded in Table 3, the rise in the ion fluence from $3x10^{16}$ ions/cm^2 to $9x10^{16}$ ions/cm^2, the γ_s^p enhanced respectively from 12.24 to 18.06 mJ/m^2, and γ_s^d from 29.20 to 37.91 mJ/m^2, and γ_s^t from 41.45 to 55.97 mJ/m^2. This indicates that the activation of the nanocomposite surface is proportional to the ion irradiation [34, 35].

Table 3. The dispersive, polar, and total surface energies (γ_s^t) for PVA/TiO_2 at different fluencies.

The samples	Dispersive γ_s^d (mJ/m^2)	Polar γ_s^p(mJ/m^2)	Total γ_s^t (mJ/m^2)
PVA/TiO_2	24.37	9.76	34.13
$3x10^{16}$ ions.cm^{-2}	29.20	12.24	41.45
$6x10^{16}$ ions.cm^{-2}	34.01	14.34	48.36
$9x10^{16}$ ions.cm^{-2}	37.91	18.06	55.97

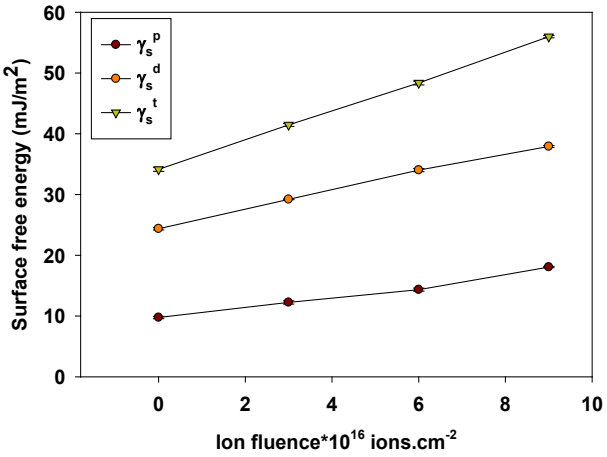

Fig. 8. Polar, dispersive and total free energies of PVA/TiO₂ at different ion fluencies.

The conductivity σ_{ac} is estimated by [36].

$$\sigma_{ac} = 2\pi f \varepsilon_o \varepsilon'' \tag{8}$$

f is frequency, ε" is dielectric loss, and ε_o is space permittivity. The σ_{ac} of both irradiated and pure PVA/TiO_2 films changes with frequency in the range of 50Hz to 5MHz is illustrated in Figure 9. Notably, the σ_{ac} rises with frequency across all samples, due to the charge carriers. By increasing ion irradiation, the conductivity at frequency 50 Hz, is enhanced from 0.32x10^{-6} S/cm for PVA/TiO_2, then 0.69x10^{-6} S/cm for 3x10^{16} ions/cm^2, and to 1.7x10^{-6} S/cm for 6x10^{16} ions/cm^2 and finally reached to 4.3x10^{-6} S/cm for 9x10^{16} ions/cm^2. This because the ion irradiations, which increases the speed of chain scissoring, is processing this rise in charge carriers [37].

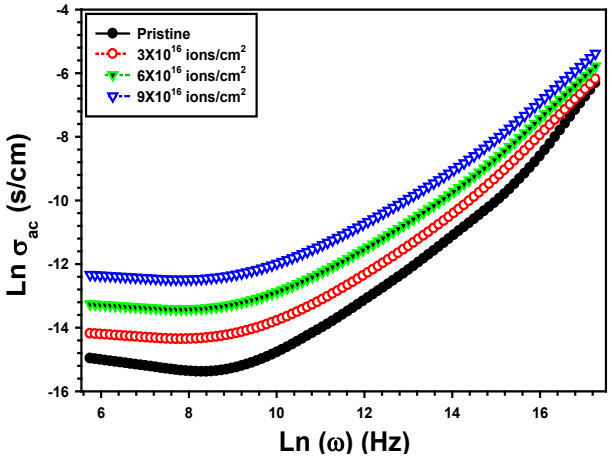

Fig. 9. σ_{ac} with frequency at different ion fluencies for PVA/TiO_2 films.

The next relation is applied to compute the maximum height potential barrier W_m [38].

$$W_m = \frac{-4k_BT}{m} \tag{9}$$

The T is the temperature, k_B is the Boltzmann constant and m is determined using the next formula [39] as illustrated in Figure 10.

$$\varepsilon'' = A\omega^m \tag{10}$$

For pure PVA/TiO_2, the computed W_m decreased to 1.07 eV, 1.06 eV for 3x10^{16} ions/cm^2, 1.05 eV for 6x10^{16} ions/cm^2, and 1.04 eV for 9x10^{16} ions/cm^2. The generated defects in the polymeric chain's composite structure caused by ion irradiation are the cause of the variations in potential barrier energy W_m [40].

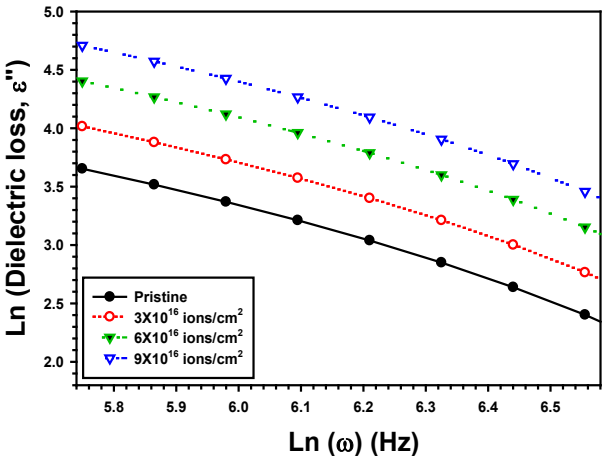

Fig. 10. Ln (ε'') versus Ln (ω) for PVA/TiO_2 at different ion fluencies.

4. Conclusions

Nanocomposites of flexible PVA and TiO_2 polymers were created by the preparation casting solution method. The AFM, XRD and SEM techniques were proved the successful preparations of the PVA/TiO_2 composite. The homemade ion sources with varying ion fluencies were used to irradiate the samples. The work of adhesion and surface energy were estimated by determine the contact angle value. The polar energy is raising from 12.24 to 18.06 mJ/m^2, and the dispersion energy is elevated of 29.20 to 37.91 mJ/m^2 by enhancing fluence of 3x10^{16} ions/cm^2 to 9x10^{16} ions/cm^2. Surface adhesion between PVA and TiO_2 is enhanced by irradiation, which forms a cohesive bond on the PVA/TiO_2 chain. Ion beams also enhanced the surface energy of PVA/TiO_2 by activating its hydrophilicity and surface polarity. Additionally, by exposing them to oxygen ion beams of varying fluencies, their electrical conductivity was enhanced. The obtained results demonstrate that the irradiated samples have a wide range of possible dielectric applications.

Acknowledgements

Princess Nourah bint Abdulrahman University Researchers Supporting Project number (PNURSP2024R399), Princess Nourah bint Abdulrahman University, Riyadh, Saudi Arabia.

References

[1] Althubiti NA, Atta A, Alotaibi BM, Abdelhamied MM (2022), Surface Innovations 11(3): 1-11; https://doi.org/10.1680/jsuin.22.00010

[2] Alotaibi BM, Al-Yousef HA, Alsaif NA, Atta A. (2022), Surface Innovations 11(3), 1-13; https://doi.org/10.1680/jsuin.22.00026

[3] Atta A, Abdelhamied MM, Abdelreheem AM, Berber MR (2021), Polymers 13(8): 1225; https://doi.org/10.3390/polym13081225
[4] Abdelhamid MM, Atta A, Reheem AM, Ashour AH (2022), Surface Innovations 11(5):1-10; https://doi.org/10.1680/jsuin.22.01004
[5] Atta A (2020), Surface Innovations 9(1): 17-24; https://doi.org/10.1680/jsuin.20.00020
[6] Atta A, Alotaibi BM, Abdelhamied MM (2022), Inorganic Chemistry Communications 141:109502; https://doi.org/10.1016/j.inoche.2022.109502
[7] Al-Yousef HA, Atta MR, Abdeltwab E, Atta A, Abdel-Hamid MM (2023), Emerging Materials Research 40: 1-13; https://doi.org/10.1680/jemmr.22.00199
[8] Atta A, Abdelhamied MM, Abdelreheem AM, Althubiti NA (2022), Inorganic Chemistry Communications 135:109085; https://doi.org/10.1016/j.inoche.2021.109085
[9] Atta A, Abdeltwab E (2022), Brazilian Journal of Physics 52(1) :1-10; https://doi.org/10.1007/s13538-021-01011-5
[10] Abdelhamied MM, Atta A, Abdelreheem AM, Farag ATM, El Sherbiny MA (2021), Inorganic Chemistry Communications 133: 108926; https://doi.org/10.1016/j.inoche.2021.108926
[11] Alotaibi, BM, Atta A, Atta MR, Abdeltwab E, Abdel-Hamid MM (2023), Surface Innovations,12(1-2):73-83; https://doi.org/10.1680/jsuin.22.01089
[12] Alotaibi BM, Atta MR, Abdeltwab E, Atta A, Abdel-Hamid MM (2023), Surface Innovations, 12(1-2):84-95; https://doi.org/10.1680/jsuin.22.01078
[13] Abdel-Galil A, Atta A, Balboul MR (2020), Surface Review and Letters 27(12): 2050019; https://doi.org/10.1142/S0218625X20500195
[14] Alsaif NA, Atta A, Abdeltwab E, Abdel-Hamid MM (2023), Surface Innovations:1-10.
[15] Atta A, Althubiti NA, Althubiti S (2021), Journal of the Korean Physical Society 79: 386-394; https://doi.org/10.1007/s40042-021-00224-w
[16] Abdeltwab E, Atta A (2021), Surface Innovations 10 (4-5): 289-297; https://doi.org/10.1680/jsuin.21.00045
[17] Atta A, Abdel Reheem AM, Abdeltwab E (2020), Surface Review and Letters 27(09): 1950214; https://doi.org/10.1142/S0218625X19502147
[18] Lotfy S, Atta A, Abdeltwab E (2018), Journal of Applied Polymer Science 135(15): 46146; https://doi.org/10.1002/app.46146
[19] Atta A, Lotfy S, Abdeltwab E (2018); Journal of Applied Polymer Science 135(33): 46647; https://doi.org/10.1002/app.46647
[20] Abdelhamied MM, Atta A, Abdelreheem AM, Farag ATM, El Okr MM (2020), Journal of Materials Science: Materials in Electronics 31(24) : 22629-22641; https://doi.org/10.1007/s10854-020-04774-w
[21] Atta A, Abdel-Hamid HM, Fawzy YHA, El-Okr MM (2019), Emerging Materials Research 8(3):354-359; https://doi.org/10.1680/jemmr.19.00054
[22] Ziegler JF, Ziegler MD, Biersack JP (2010), Nuclear Instruments and Methods in Physics Research Section B: Beam Interactions with Materials and Atoms 268(11-12): 1818-1823; https://doi.org/10.1016/j.nimb.2010.02.091
[23] Gavade C, Singh NL, Khanna PK (2014), Journal of nanoscience and nanotechnology 14(8): 5911-5916; https://doi.org/10.1166/jnn.2014.8736
[24] Aziz SB, Brza MA, Mohamed PA et al. (2019), Results in Physics 13: 102326; https://doi.org/10.1016/j.rinp.2019.102326
[25] Fawzy YHA, Abdel-Hamid HM, El-Okr MM, Atta A (2018), Surface Review and Letters 25(03): 1850066; https://doi.org/10.1142/S0218625X1850066X
[26] Abdel-Galil A, Ali HE, Atta A, Balboul MR (2014), Journal of Radiation Research and Applied Sciences 7(1) :36-43; https://doi.org/10.1016/j.jrras.2013.11.004
[27] Atta, A., Fawzy, Y. H., Bek, A., Abdel-Hamid, H. M., El-Oker, M. M. (2013). Nuclear Instruments and Methods in Physics Research Section B: Beam Interactions with Materials and Atoms, 300, 46-53; https://doi.org/10.1016/j.nimb.2013.02.004

[28] Papakonstantinou, D., Amanatides, E., Mataras, D., Ioannidis, V., Nikolopoulos, P. (2007), Plasma Processes and Polymers, 4(S1), S1057-S1062; https://doi.org/10.1002/ppap.200732405

[29] Abdeltwab, E., Atta, A. (2022), ECS Journal of Solid State Science and Technology, 11(4), 043012; https://doi.org/10.1149/2162-8777/ac66fe

[30] Owens, D. K., Wendt, R. C. (1969), Journal of applied polymer science, 13(8), 1741-1747; https://doi.org/10.1002/app.1969.070130815

[31] Meuler, A. J., Chhatre, S. S., Nieves, A. R., Mabry, J. M., Cohen, R. E., McKinley, G. H. (2011), Soft Matter, 7(21), 10122-10134; https://doi.org/10.1039/c1sm05994g

[32] Atta, A., Abdeltwab, E. (2022), Brazilian Journal of Physics, 52(1), 1-10; https://doi.org/10.1007/s13538-021-01011-5

[33] Ainali, N. M., Bikiaris, D. N., Lambropoulou, D. A. (2021), Journal of Analytical and Applied Pyrolysis, 158, 105207; https://doi.org/10.1016/j.jaap.2021.105207

[34] Ahmed H, Hashim A, Egyptian Journal of Chemistry (2020) 63:805-811.

[35] Ebrahim S, Kashyout AH, Soliman M, Current Applied Physics (2009) 9: 448-454; https://doi.org/10.1016/j.cap.2008.04.007

[36] Bouaamlat H, Hadi N, Belghiti N, Dielectric properties, Advances in Materials Science and Engineering. (2020) 20: 1-8; https://doi.org/10.1155/2020/8689150

[37] Hashim A, Hadi A, Ukrainian Journal of Physics (2018) 63, 754-754; https://doi.org/10.15407/ujpe63.8.754

[38] Abdeltwab E, Atta A, International Journal of Modern Physics (2021) B 35: 2150310; https://doi.org/10.1142/S0217979221503100